Supporting Information

Fine Tuning of Electrical Characteristics of Inkjet Printed Graphene for Physical and Chemical Sensing

Hyun-June Jang[1,2], Rapti Ghosh[1,2], Wen Zhuang[1,2], Xiaoben Zhang[1,2], Yuqin Wang[1,2], Xiaoao Shi[1,2], Xingkang Huang[1,2], *Haihui Pu[1,2], Byunghoon Ryu[3], Janan Hui[4], Mark C. Hersam[4,5,6], Junhong Chen[1,2*]*

[1]Pritzker School of Molecular Engineering, University of Chicago, Chicago, IL 60637, USA

[2]Chemical Sciences and Engineering Division, Physical Sciences and Engineering Directorate, Argonne National Laboratory, Lemont, IL 60439, USA

[3]Department of Mechanical Engineering, Inha University, Incheon, 22212, Republic of Korea

[4]Department of Materials Science and Engineering, Northwestern University, Evanston, IL 60208, USA

[5]Department of Chemistry, Northwestern University, Evanston, IL 60208, USA

[6]Department of Electrical and Computer Engineering, Northwestern University, Evanston, IL 60208, USA

*Correspondence: junhongchen@uchicago.edu

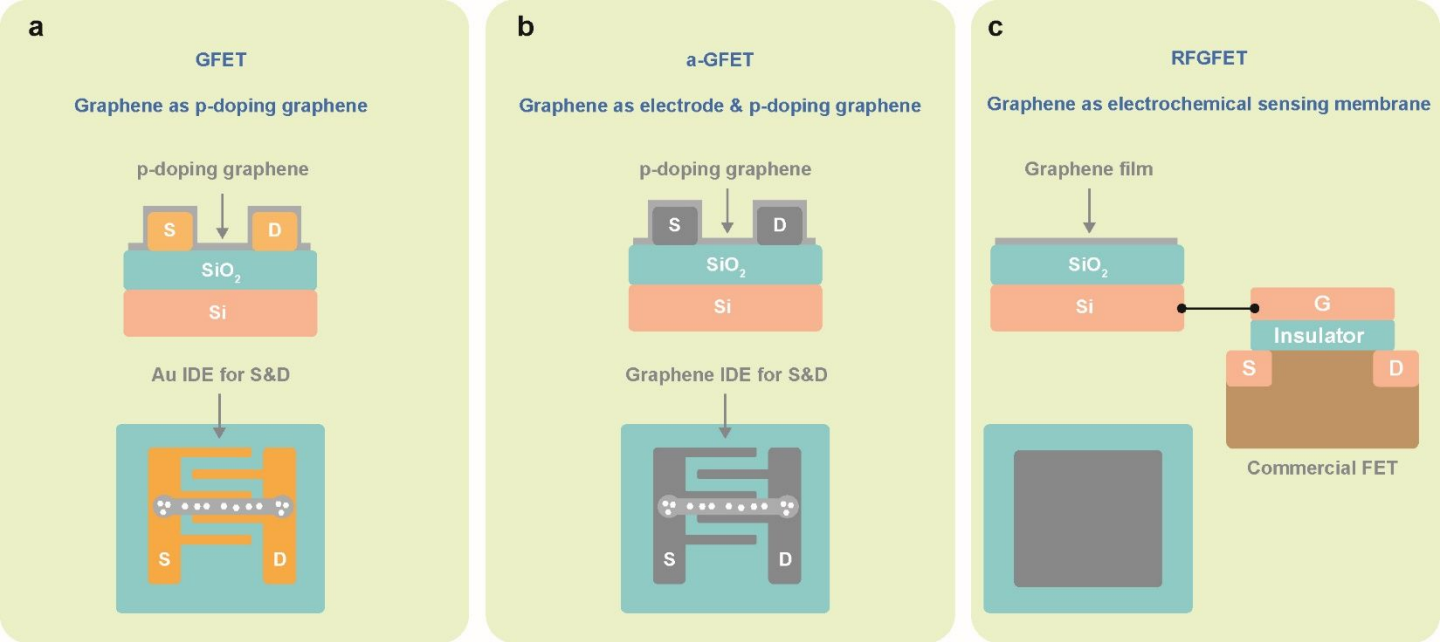

Figure S1. Schematic diagrams of the device structures (cross-sectional and plan views) are shown for (a) GFET, (b) a-GFET, and (c) RFGFET. Inkjet-printed graphene/EC is used as p-doped graphene in the GFET design (Figure S1a). Two distinct Au IDE designs were prepared for Figure S1a, with the width, spacing, and length of each finger being 2/2.5/780 μm and 5/7.5/700 μm, respectively. In the a-GFET (Figure S1b), p-doped graphene/EC was used for the channel, while low-resistance graphene/EC was applied to the IDE. The graphene IDE had finger dimensions of 100/100/800 μm (width/spacing/length). Finally, the RFGFET in Figure S1c demonstrates graphene used for an electrochemical sensing membrane.

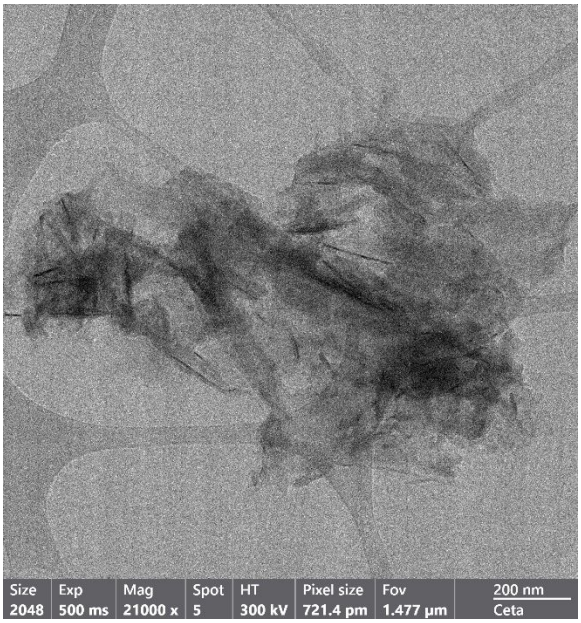

Figure S2. TEM image of the graphene/EC nano flake.

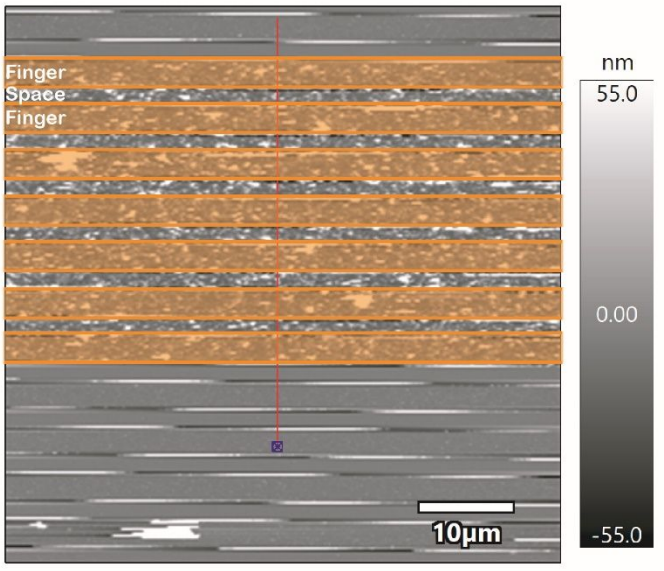

Figure S3. AFM image of the graphene/EC network printed over Au IDE fingers, with a spacing of 2 µm between the fingers.

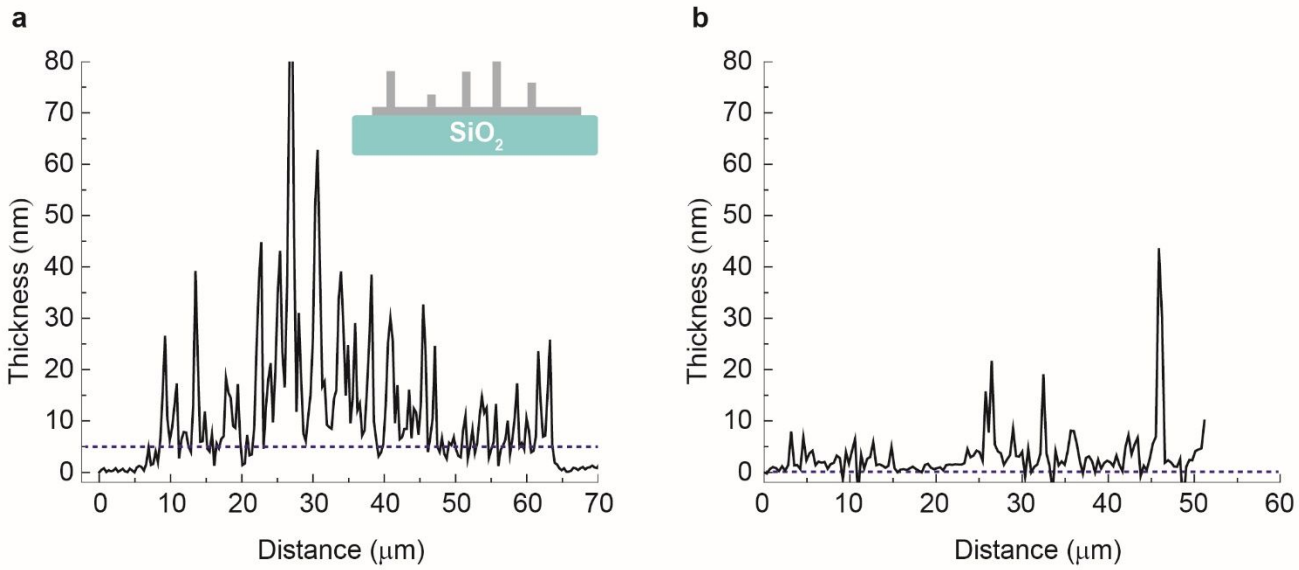

Figure S4. The atomic force microscopy (AFM) surface profile analysis presented herein focuses on two distinct inkjet-printed graphene/EC configurations on SiO_2 substrates. (a) The surface profile of graphene/EC deposited in a circular shape after annealing at 200 ºC, where the observed roughness is approximately 15 nm. (b) A continuous graphene film formed between IDE fingers after annealing at 200 ºC, showcasing a significantly smoother surface with a roughness measured at about 6.67 nm.

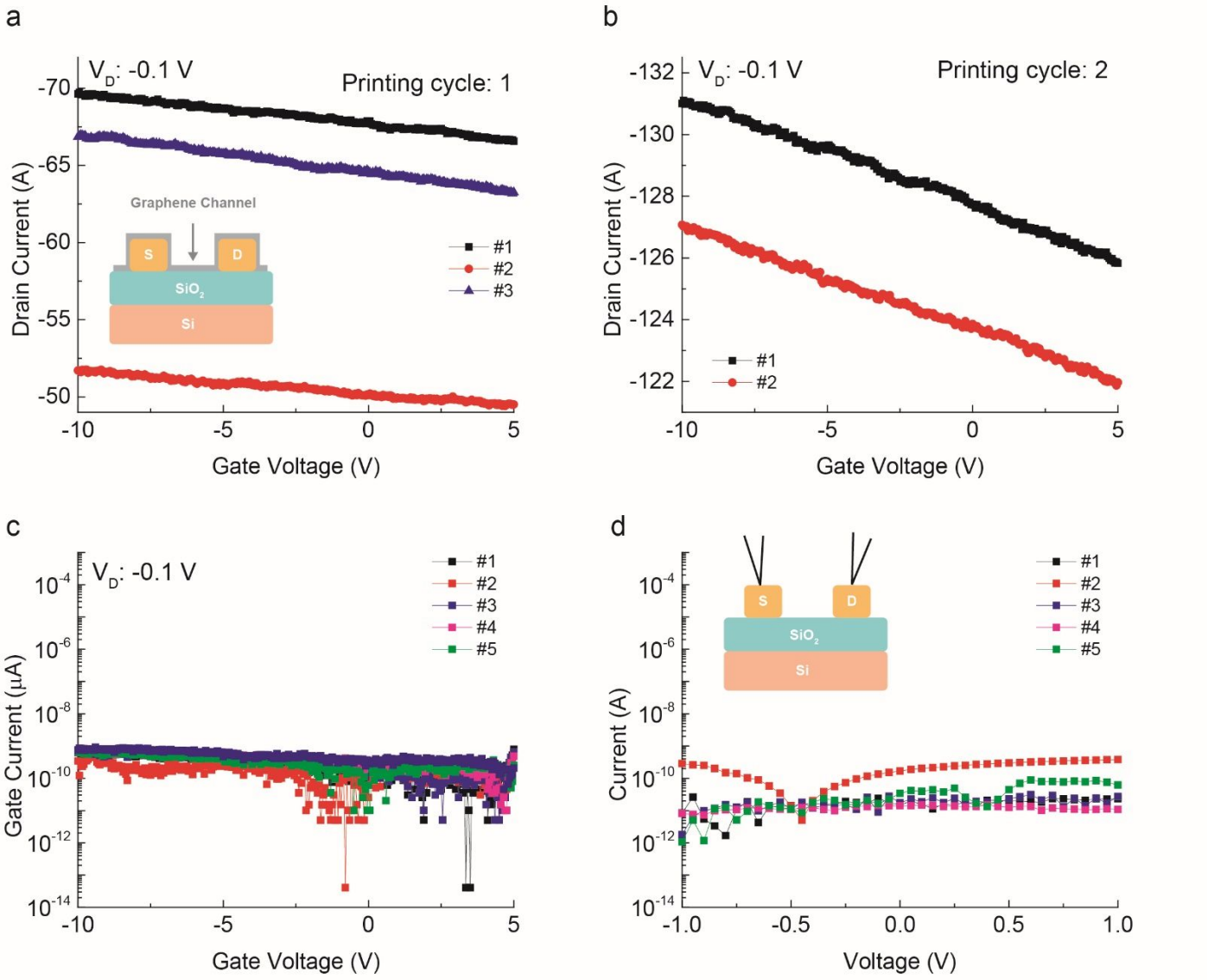

Figure S5. The transfer curves of GFETs with varying layers of printed graphene on Au IDEs are examined in detail. (a) Transfer curves of GFETs with a single layer of printed graphene and (b) those with two layers, both annealed at 200 ºC. The gate current of GFETs with (c) double layers of printed graphene/EC and (d) leakage current components measured from IDEs without printed graphene/EC.

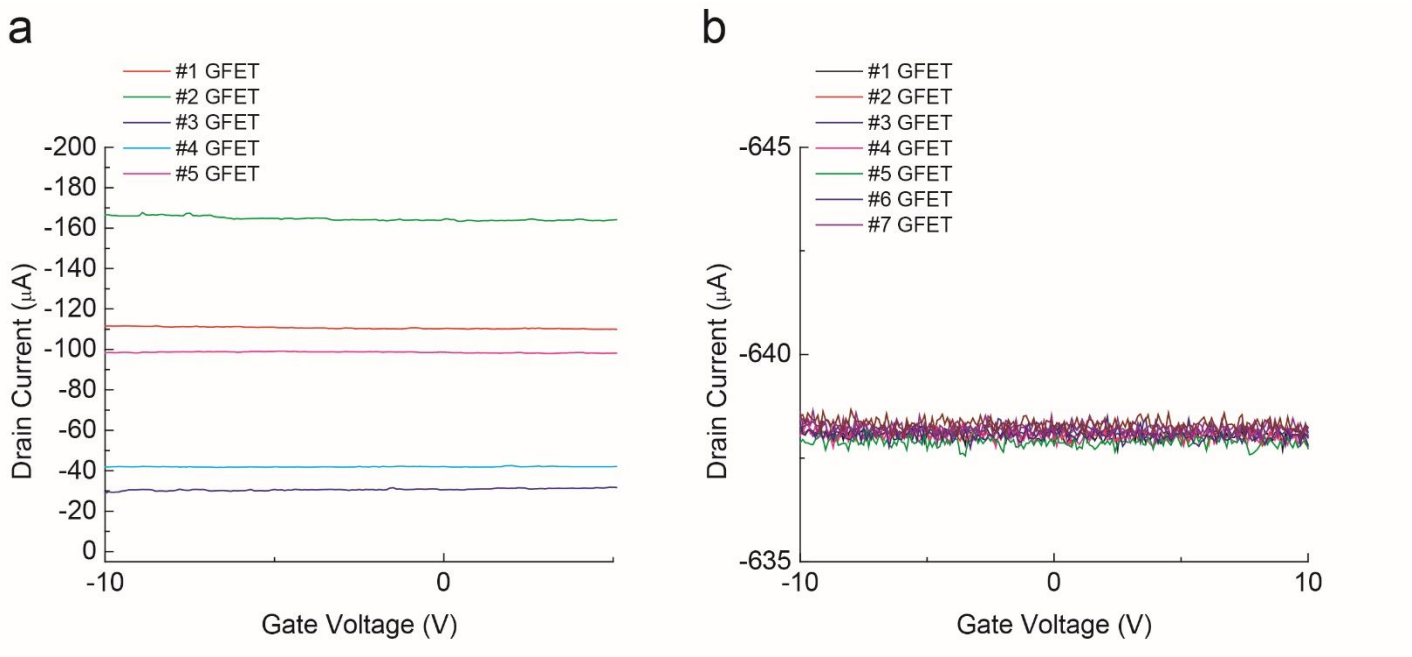

Figure S6. Transfer curves of GFETs fabricated on Au IDEs with a 5-μm spacing between the fingers, using graphene/EC annealed at (a) 200 °C and (b) 400 °C. Five and seven different GFETs were measured, respectively.

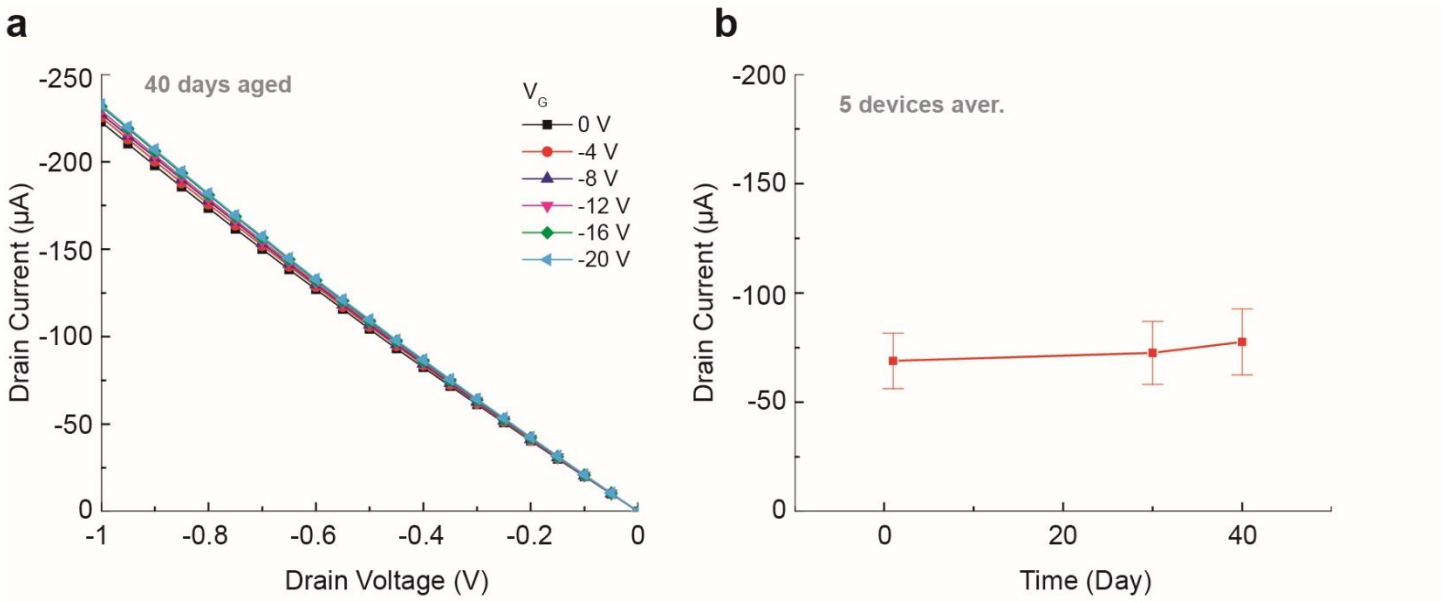

Figure S7. (a) Output curves of a GFET annealed at 200 ºC, measured 40 days post-fabrication, and (b) the drain current levels of five different GFETs, recorded at a gate voltage of -0.5 V, illustrating how they varied over time.

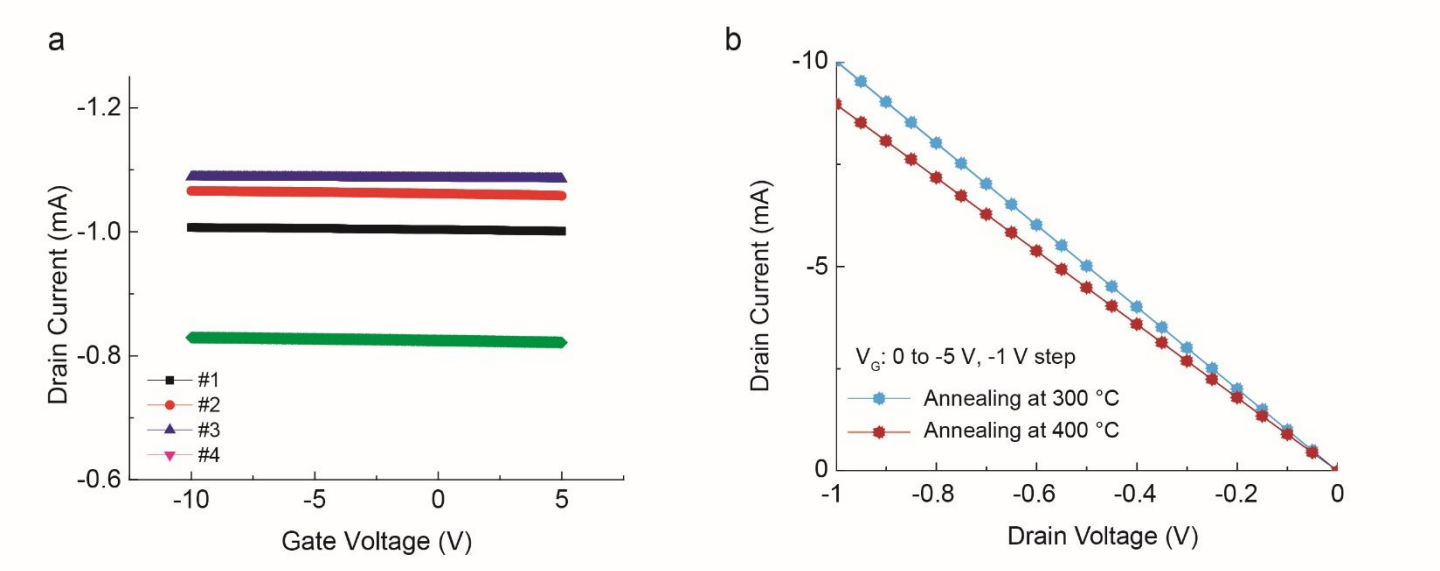

Figure S8. (a) Transfer curves of four different GFETs annealed at 300 ºC, exhibiting conductive properties without gate modulation effects. (b) Output curves of GFETs annealed at 300 ºC and 400 ºC.

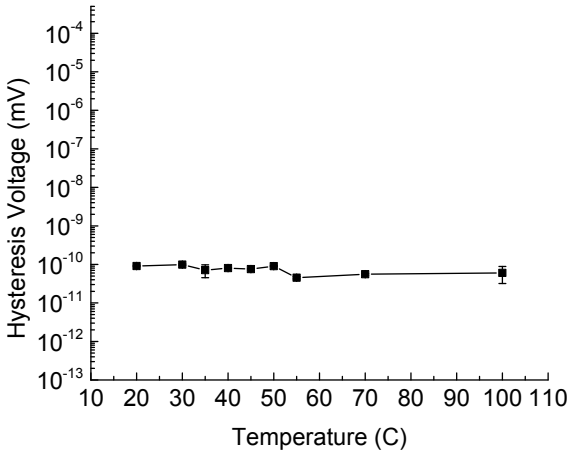

Figure S9. The correlation between the hysteresis voltage measured from the transfer curves of GFET annealed at 200 ºC in double-sweeping mode and the hot plate temperature where the GFET is placed. The hysteresis voltage remains below 1 nA across the entire temperature range. This indicates that the interface traps between graphene/EC and SiO_2 have an insignificant effect. The bell-shaped response curve in Figure 2c primarily reflects the intrinsic temperature response of the graphene/EC channel in the GFET, suggesting that lattice vibrations (phonons) and scattering mechanisms may become dominant within the GFET channel.

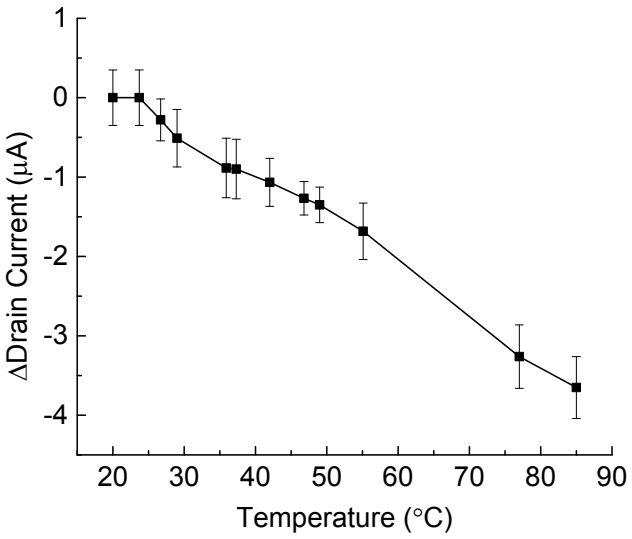

Figure S10. The relationship between temperature applied to GFETs and the change in drain current of GFETs annealed at 400 ºC. Measurements were conducted on three different GFETs.

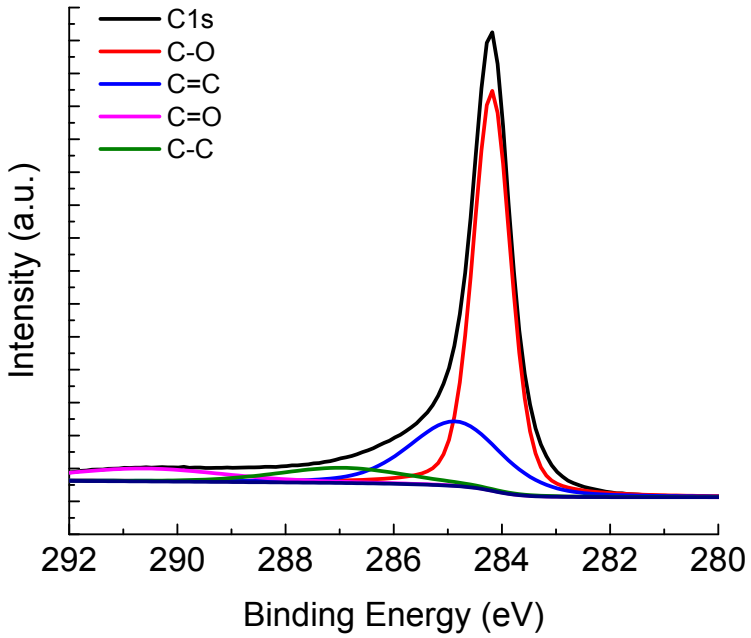

Figure S11. XPS data for a graphene/EC film annealed at 400 ºC.

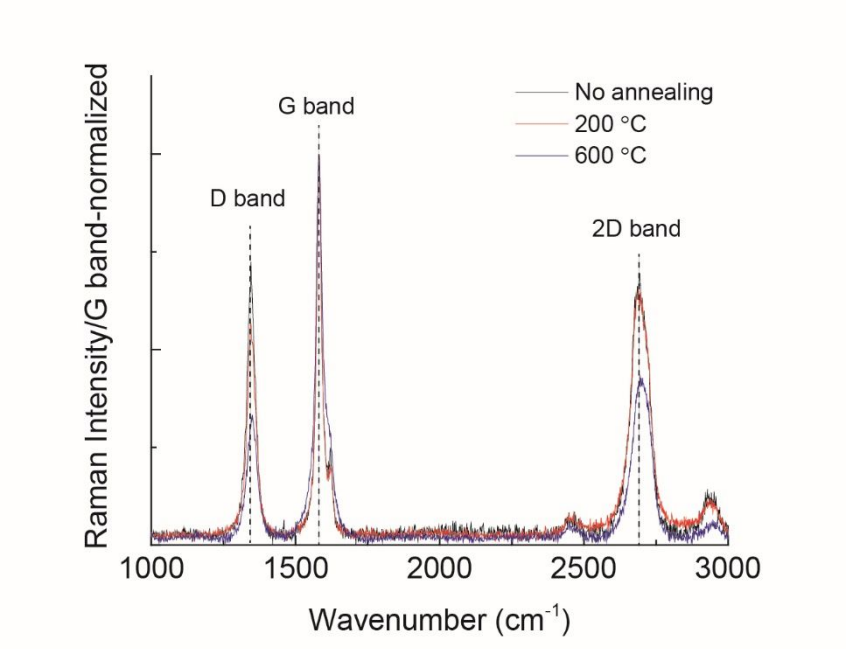

Figure S12. Raman spectra of graphene/EC annealed at different temperatures. Raman analysis indicated a reduction in oxygen-functional groups with increasing annealing temperature, as reflected by the I_D/I_G ratios of 0.71, 0.55, and 0.32 for graphene/EC without annealing, annealed at 200 ºC, and annealed at 600 ºC, respectively, and I_{2D}/I_G ratios of 0.68, 0.65, and 0.42 for the same conditions.

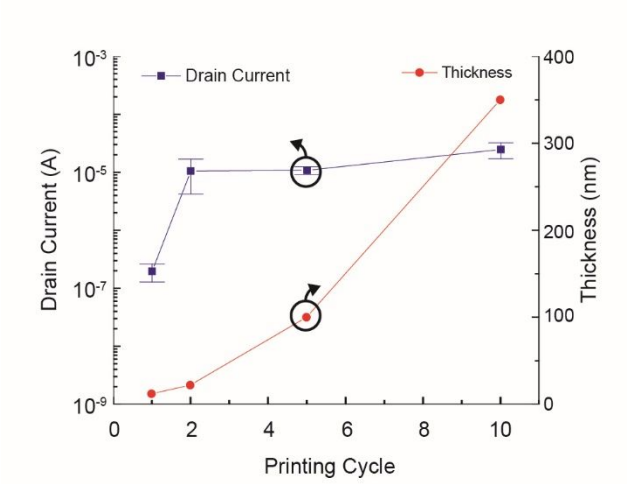

Figure S13. The drain current levels of inkjet-printed GFETs with varying number of graphene printing layers for each channel. The original graphene/EC ink was diluted by 50% to precisely control the thickness of these printed layers. AFM was used to measure the thickness of each printing layer. The results show that the average thickness of the edge area of the graphene film varied depending on the number of printing cycles: 12 nm for 1 cycle, 22 nm for 2 cycles, 100 nm for 5 cycles, and 350 nm for 10 cycles.

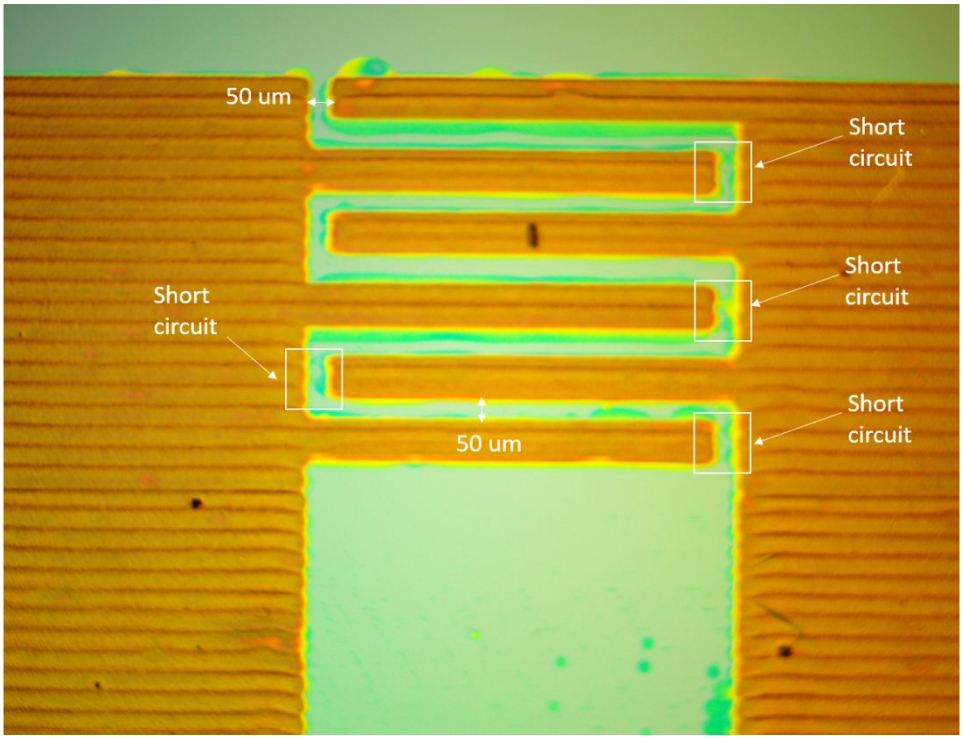

Figure S14. Microscopy image of graphene/EC IDE annealed at 350 ºC.

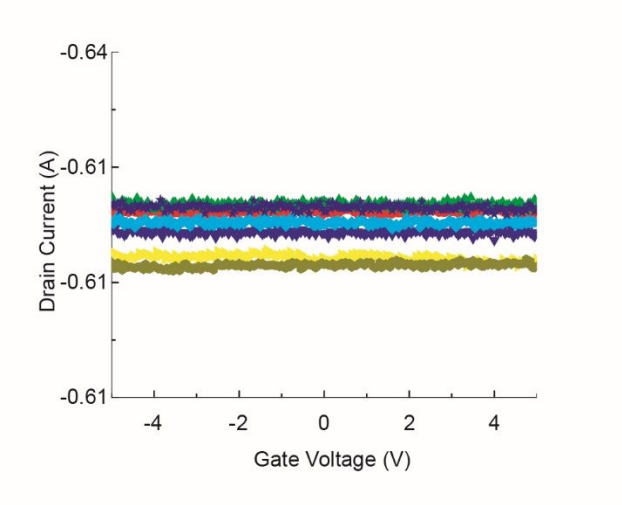

Figure S15. Transfer curves of eight a-GFET devices annealed at 350 ºC.

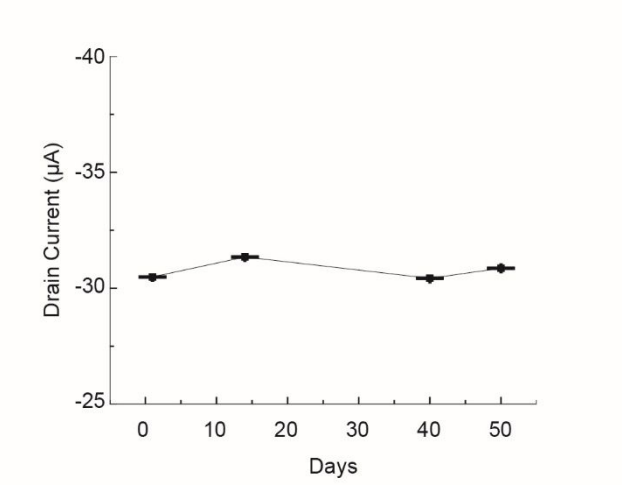

Figure S16. Drain current changes of 5 different all inkjet-printed GFETs devices annealed at 200 ºC over time.

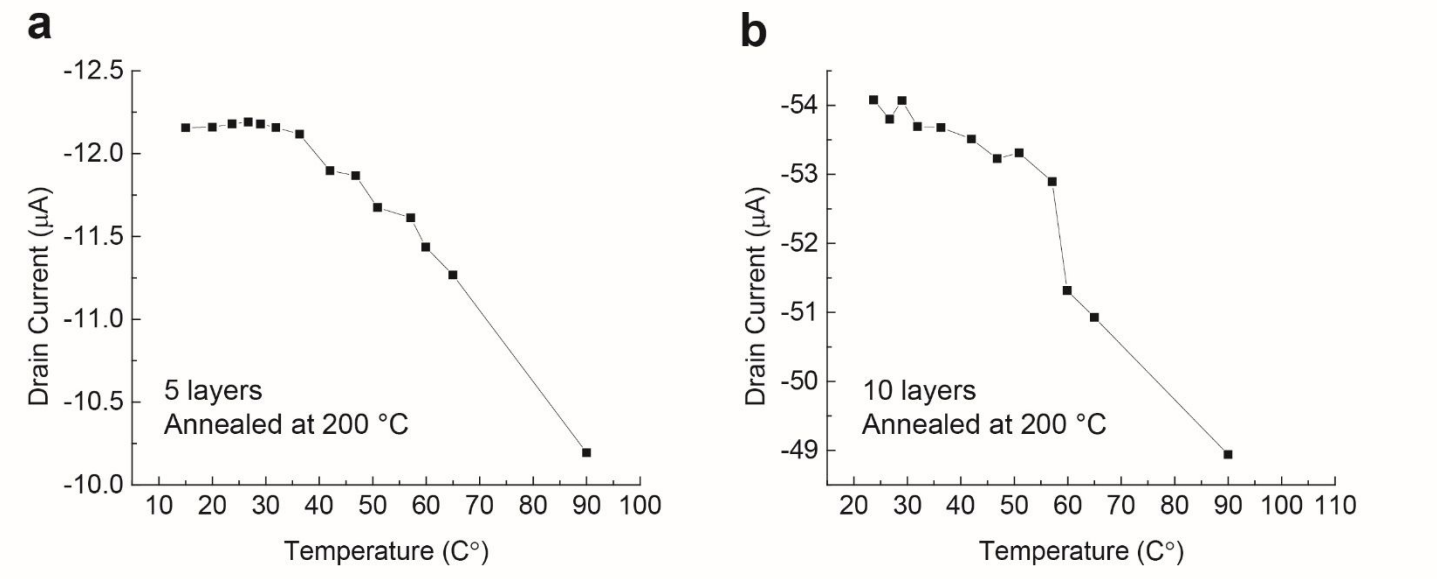

Figure S17. The variations in drain current as a function of temperature for all inkjet-printed GFET devices, showcasing two different configurations: devices with (a) 5 layers and (b) 10 layers of inkjet-printed graphene/EC. Both configurations were annealed at 200 ºC.

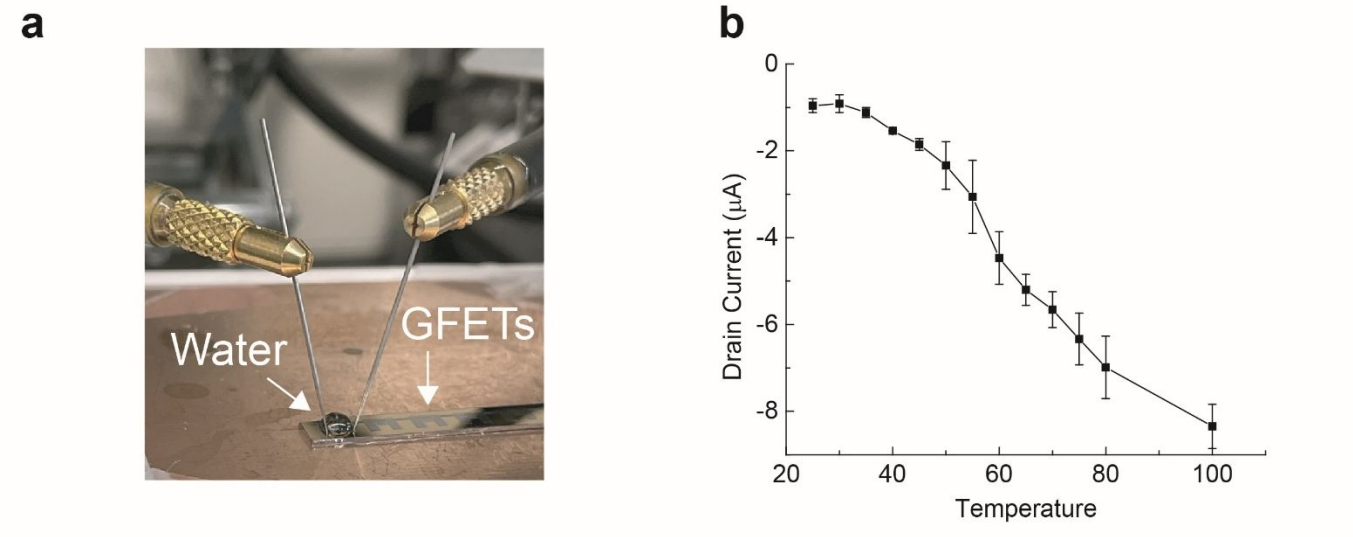

Figure S18. (a) Measurement setup for temperature detection in water: Initially, 40 µL of water was applied to the GFET channel area, which suffices to fully cover the graphene channel. As the water evaporated due to heating, additional water was added to ensure the channel remained fully covered throughout the experiment. (b) Drain current changes of GFETs measured in the setup described in Figure S11a as a function of temperature: The GFETs, annealed at 400 ºC, exhibited a decrease in drain current with increasing hot plate temperature, deviating from the bell-shaped curve, as shown in Figure 2c.

a

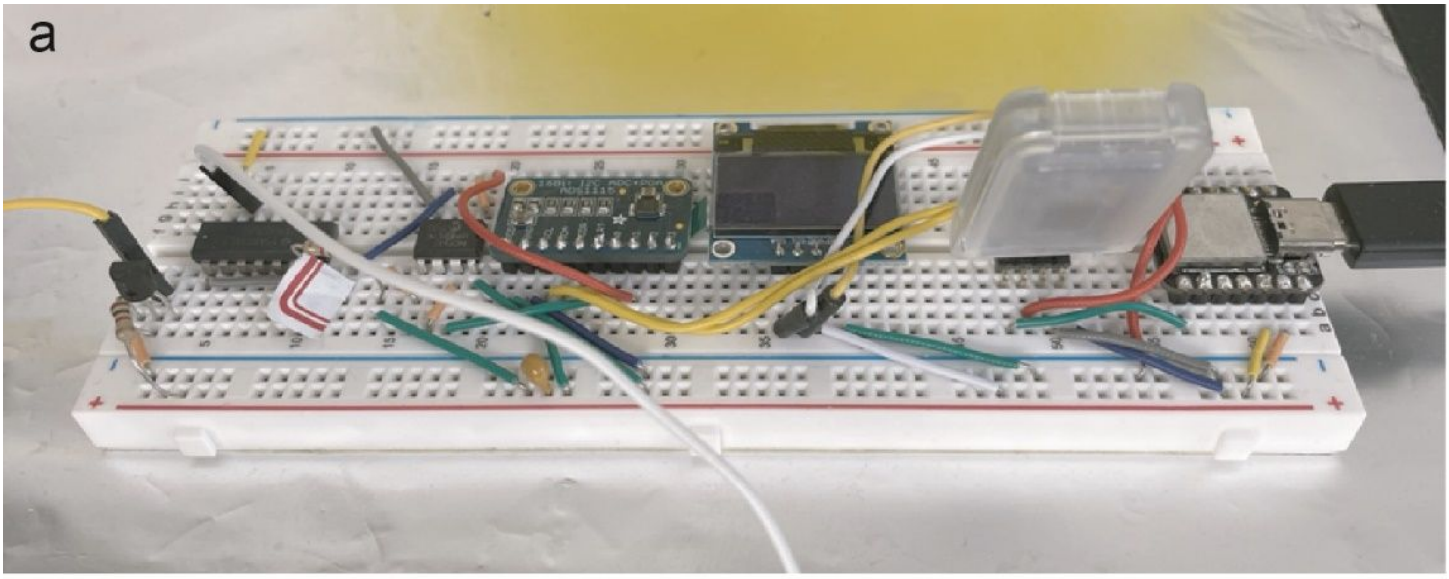

b

Reader Device

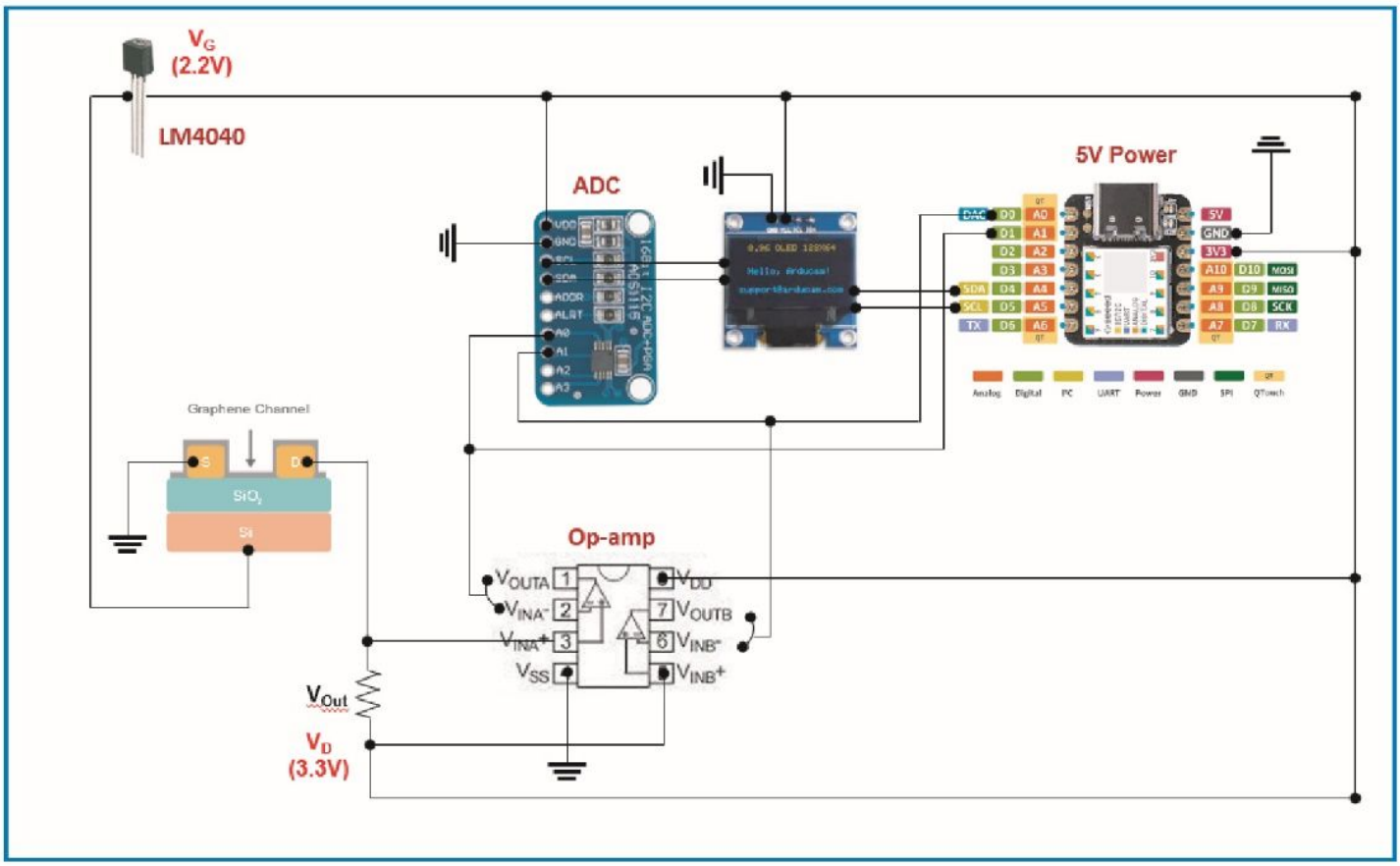

Figure S19. Handheld device components for temperature sensors are illustrated as follows: (a) An actual photo displaying the handheld temperature device constructed on a breadboard. (b) A schematic depicting the essential components required for the handheld temperature sensors. The all inkjet-printed GFET is positioned on a hot plate for measurement in Figure 3a.

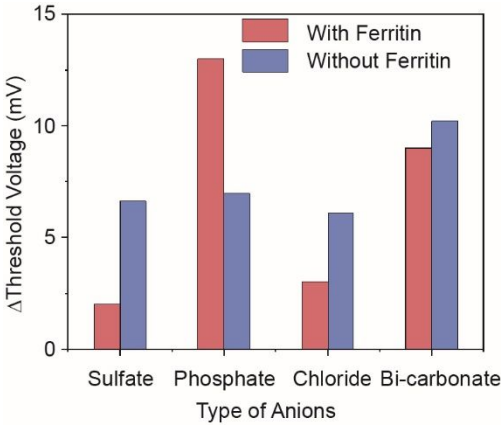

Figure S20. Selectivity tests conducted on graphene/EC film in a remote floating-gate structure, both with and without ferritin probe functionalization, where the setup without the ferritin probe served as the control. Various anions, including sulfate, chloride, and bicarbonate, were tested. Sample solutions at concentrations of 100 ng/mL and 1 µg/mL, with DI water as the solvent, were prepared and measured on graphene/EC film functionalized with ferritin to assess ΔV_{th}, referred to as ΔV_{th} with ferritin. ΔV_{th} was defined as the difference in V_{th} between analyte solutions at concentrations of 100 ng/mL and 1 µg/mL in DI water. Due to the influence of anion concentration on pH, ΔV_{th} between 100 ng/mL and 1 µg/mL was also measured for bare graphene/EC film (without ferritin) to account for pH-related ΔV_{th} changes, referred to as ΔV_{th} without ferritin. For phosphate, ΔV_{th} with ferritin was greater than ΔV_{th} without ferritin, indicating ferritin's high selectivity for phosphate detection.

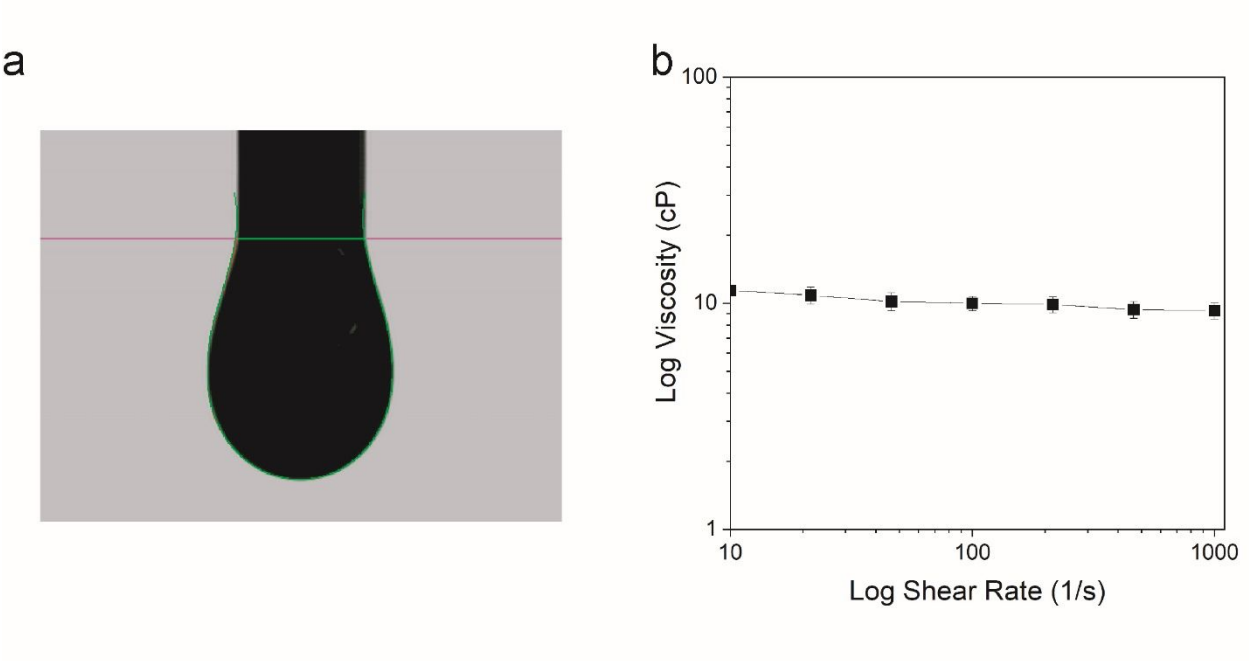

Figure S21. (a) Surface tension image, and (b) viscosity versus shear rate, measured at room temperature using an Anton Paar Physica MCR 302 rheometer equipped with a CP 25-2 fixture and Peltier plate.